

Identifying Multi-modal Knowledge Neurons in Pretrained Transformers via Two-stage Filtering

Yugen Sato

Meiji University

Kanagawa, Japan

yugen0104.tu@gmail.com

Tomohiro Takagi

Meiji University

Kanagawa, Japan

takagit@gmail.com

Abstract—Recent advances in large language models (LLMs) have led to the development of multimodal LLMs (MLLMs) in the fields of natural language processing (NLP) and computer vision. Although these models allow for integrated visual and language understanding, they present challenges such as opaque internal processing and the generation of hallucinations and misinformation. Therefore, there is a need for a method to clarify the location of knowledge in MLLMs.

In this study, we propose a method to identify neurons associated with specific knowledge using MiniGPT-4, a Transformer-based MLLM. Specifically, we extract knowledge neurons through two stages: activation differences filtering using inpainting and gradient-based filtering using GradCAM. Experiments on the image caption generation task using the MS COCO 2017 dataset, BLEU, ROUGE, and BERTScore quantitative evaluation, and qualitative evaluation using an activation heatmap showed that our method is able to locate knowledge with higher accuracy than existing methods.

This study contributes to the visualization and explainability of knowledge in MLLMs and shows the potential for future knowledge editing and control.

I. INTRODUCTION

In recent years, the advancement of large language models (LLMs) has established them as foundational models for numerous applications in the field of natural language processing (NLP). Inspired by this success, researchers in computer vision have extended the input modality of language models, leading to the development of multimodal large language models (MLLMs) capable of processing both text and images. MLLMs provide an integrated understanding of vision and language, achieving remarkable performance improvements in tasks such as image captioning and visual question answering (VQA).

One of the key underlying technologies contributing to the success of LLMs and MLLMs is the Transformer [1]. While the Transformer has revolutionized machine learning and contributed to performance improvements across various fields, its internal processes remain largely opaque, limiting its interpretability. In particular, for text generation models such as LLMs and MLLMs, this opacity can lead to unintended outputs, including the generation of harmful or misleading content [2] and hallucinations [3]. These issues highlight the urgent need to enhance model interpretability, not only for a deeper understanding of these models but also for ensuring responsible and ethical applications.

Improving interpretability would enable the identification and localization of knowledge within the Transformer, allowing for

the modification or removal of specific knowledge to facilitate controlled model development and adaptation. This flexibility would significantly contribute to the refinement and responsible use of Transformer-based models.

In this study, as a first step toward enhancing the interpretability of Transformer-based text generation models, we conduct neuron-level observations using MiniGPT-4 [4] to clarify the localization of knowledge.

Several studies have approached similar challenges [5]–[7]. Research on MLLMs often emphasizes neurons that bridge textual and visual features. Notably, Schwettmann et al. [5] extended this concept by identifying multimodal neurons even in purely textual components of LLMs, revealing their ability to bridge visual and textual representations. Additionally, Pan et al. [6] proposed a method that scores neurons based on sensitivity, specificity, and causal effects, focusing on the final token of textual input to identify multimodal neurons associated with specific visual knowledge.

However, their approach primarily analyzes the influence of language tokens and does not directly elucidate how MLLMs internally retain and process knowledge through visual features. Existing methods rely on model-driven techniques based on internal representations and weights, while data-driven approaches that observe internal representations under varying input conditions remain largely unexplored.

To address this gap, we propose a data-driven approach that leverages the multimodal nature of MLLMs by analyzing neuron activations and gradients at image token positions within the input sequence. To demonstrate that the identified neurons are associated with target knowledge, we conduct text generation experiments with noise perturbation using the MS COCO dataset [8].

Our contributions can be summarized as follows:

- We propose a novel method for identifying knowledge neurons in Transformer-based MLLMs.
- Through image caption generation experiments with noise perturbation and additional analyses, we demonstrate that the identified neurons are related to specific target knowledge.

II. METHOD

In this study, we first describe the architecture and model of the MLLMs used (§II-A), then define neurons in the Transformer (§II-B), and finally explain our method for identifying knowledge neurons (§II-C).

A. Multimodal Large Language Models

MLLMs are generally composed of an image encoder, a linear layer, and an LLM. The image encoder receives an image, divides it into several small image patches, and extracts image features as output. The output of the image encoder is represented as $\mathcal{F} \in R^{P \times d_h}$, where P is the number of image patches and d_h is the hidden size of the image encoder. The image features \mathcal{F} are aligned with text embeddings through a linear layer, and using the hidden size h of the LLM, they are transformed into $\mathcal{F}' \in R^{P \times h}$. Finally, the image features are concatenated with text prompt embeddings and fed into the LLM.

1) *Architecture of MLLMs*: According to Jin et al. [9], a typical MLLM consists of three main modules: a visual encoder, a pretrained language model, and a vision-language projector. The vision-language projector serves as a bridge to align the two modalities, and there are two primary approaches to this alignment.

MLP-based Approach This method integrates image features into the language space using a simple learnable linear projector or a multilayer perceptron (MLP). The MLP consists of alternating linear projectors and nonlinear activation functions. MiniGPT-4, which we use in this study, adopts an MLP-based architecture.

Attention-based Approach BLIP2 [10] introduced a lightweight Transformer module called Q-Former, which uses learnable query vectors to extract visual features from a frozen vision model. Additionally, Flamingo [11] introduced the Perceiver Resampler, which utilizes learnable latent queries (Q) in cross-attention, expanding and integrating image features into key (K) and value (V) representations. This allows the Transformer output at the corresponding positions of learnable latent queries to function as an aggregated representation of visual features, enabling the standardization of variable-length video frame features into fixed-size representations.

Other Approaches Various other methods, such as CNN-based and Mamba-based approaches, have also been explored [9].

We focus our analysis on models that adopt the most common MLP-based architecture. This selection is motivated by the constraints of available models for activation heatmap generation (§V).

2) *MiniGPT-4*: MiniGPT-4 is a model designed to adapt pretrained LLMs, such as Vicuna [12] and Llama-2 [13], to image features output by using a pretrained image encoder. The image encoder used in MiniGPT-4 includes models such as BLIP2 and ViT [14].

As described in §II-A1, a bridging module is required between the image encoder and the language model. MiniGPT-4 adopts both MLP-based and attention-based approaches, which are available as separate models. In this study, we use the MLP-based model, which employs ViT as the image encoder and Llama-2 (7B) as the language model. Hereafter, we refer to this version simply as MiniGPT-4.

B. Neurons in Transformer

Typically, a decoder-only Transformer consists of stacked Attention layers and FFN layers. Each layer first applies multi-

head self-attention in the Attention layer, followed by residual connections and layer normalization. Then, an FFN layer, composed of two linear layers and an activation function, is applied.

Let h^l be the hidden state of layer l , m^l the output of the FFN layer, and a^l the output of the Attention layer. Then, m^l can be expressed as follows:

$$m^l = W_{out}^l \sigma(W_{in}^l (a^l + h^{l-1})) \quad (1)$$

where h^0 is the input embedding vector, σ is the activation function, and W_{in}^l and W_{out}^l correspond to the first and second layers of the FFN, respectively.

Attention is a crucial mechanism in the Transformer, extracting contextually relevant information and knowledge. The FFN layer was initially considered a simple nonlinear transformation. However, in 2020, Geva et al. [15] revealed that the FFN layer also plays an important role in storing knowledge and memory. Their study showed that the FFN layer functions as a key-value transformation for knowledge, where each row of the first weight matrix, W_{in}^l , acts as a key, and the columns of W_{out}^l serve as values.

This implies that when a specific key is input, it is activated by the activation function σ . The corresponding value is retrieved and then mixed into the intermediate representation through residual connections. Moreover, these value vectors often contain human-interpretable concepts and knowledge. [16]

Similarly, Meng et al. [17] investigated GPT models and measured the indirect influence of hidden states and activations on responses. They found that factual knowledge is primarily stored in the FFN layers of early model layers. Additionally, Dai et al. [18] demonstrated the existence of knowledge neurons in pretrained Transformer FFN layers through neuron-editing experiments.

Based on these insights, numerous studies have sought to elucidate the knowledge and memory functions of Transformer-based language models. [5], [6], [19] Consequently, this study, which aims to clarify the location of knowledge in Transformers, also focuses on neurons in the FFN layer.

For simplicity, we define the output of the activation function σ as $O^l = \sigma(W_{in}^l (a^l + h^{l-1}))$ and concatenate the values from all layers to obtain O . In this study, we refer to this as the activation value. Here, $O \in \mathbb{R}^{L \times T \times d_f}$, where L represents the number of model layers, T is the length of the input token sequence, and d_f is the intermediate dimension of the FFN layer. We denote the i -th neuron of the l -th layer as (Ll, Ui) and define the set of all neurons as A .

C. Identifying Knowledge Neurons

As described in II-B, previous studies have shown that activations in FFN layers are closely related to the knowledge function of Transformers. Based on this, we hypothesize that by observing activation value changes when modifying part of the input features, we can derive the relevance of those features.

Following this hypothesis, this study proposes a method that involves editing input images by removing objects associated

with specific knowledge. We then compare neuron activations before and after image modification, using GradCAM for filtering, to determine the relevance of the removed objects (knowledge).

As outlined in II-B, we focus on the activation function output O of the FFN layer. Since MiniGPT-4 inputs image features as soft prompts to the LLM, given image input img and text input $text$, the input token sequence (excluding special tokens) is represented as $(img_1, img_2, \dots, img_P, text_1, \dots, text_T)$.

Restricting the activation values to image tokens, we define $O' \in \mathbb{R}^{L \times P \times d_f}$. When targeting knowledge k associated with a specific image o , the activation values for image tokens are denoted as $O'_o{}^k$.

In the following sections, we describe the method for identifying neurons based on $O'_o{}^k$ as the starting point.

a) *Activation differences filtering using inpainting*: To generate images with specific knowledge-associated objects removed, this study employs inpainting [20]. Given an image o containing an object associated with knowledge k , we create an inpainted image i where the corresponding object has been removed. The activation values of image tokens in the inpainted image are denoted as $O'_i{}^k$.

Since the inpainting operation is restricted to the region containing the object associated with knowledge k , the resulting image appears as if only the object corresponding to knowledge k has been removed. Figure 1 illustrates an example where the knowledge target is "bear," showing both the original and inpainted images.

By computing the difference between activation values, $O'_o{}^k - O'_i{}^k$, we evaluate the neurons most relevant to the target knowledge k . Neurons with larger activation differences are considered more strongly associated with knowledge k . We define a threshold for activation differences per sample and collect neurons exceeding this threshold into a candidate set C^k .

$$C^k = \{(Ll, Ui) \in A \mid V^k[l, p, i] > threshold_a^k\}$$

Here, p denotes an image patch, and $threshold_a^k$ represents the activation differences threshold for knowledge k . A neuron is selected as a candidate if its activation differences exceed the threshold for at least one patch P .

b) *Gradient-based Filtering using GradCAM*: For neurons $(Ll, Ui) \in C^k$ obtained through II-C0a, we further refine the selection using GradCAM [21]. This step aims to eliminate neurons activated by factors unrelated to knowledge k .

First, we generate an image caption using the text prompt "The image shows a". We confirm that the generated caption contains the correct token c associated with knowledge k and use the preceding token sequence for gradient computation. Given the model's prediction logit y_c for c , the GradCAM value g_c is computed as:

$$g_c = O'_o \frac{\partial y_c}{\partial O'_o} \quad (2)$$

Similar to activation value difference filtering, we define a threshold for GradCAM values and extract neurons exceeding



Fig. 1: Original and inpainted images

the threshold from C^k to construct the final set of neurons associated with knowledge k , denoted as N_k :

$$N_k = \{(Ll, Ui) \in C^k \mid g_c[l, p, i] > threshold_g^k\}$$

Here, $threshold_g^k$ represents the GradCAM threshold for knowledge k .

III. EXPERIMENTS

A. Dataset

In this study, we utilize the 2017 train/val split of the MS COCO dataset [8]. Since MS COCO provides bounding box (BBOX) information indicating object regions in images, we leverage this data for the inpainting process described in II-C0a.

Due to the nature of our method, which relies on activation value differences, the usable data is subject to the following constraints: the generated caption for the original image must contain the target knowledge; the generated caption for the inpainted image must not contain the target knowledge; the inpainting process must remove only the target knowledge.

The MS COCO dataset provides labels for categories such as {animal, vehicle, food, ...} and specific objects such as {horse, bear, airplane, ...}. Under these constraints, we select three types of knowledge (objects) from each category and sample three instances per object, resulting in a total of 90 data samples, denoted as D , for our experiments.

B. Compared Methods

We compare our method with the approach devised by Schwettmann et al. [5] (abbreviated as Schwettmann's). Their method detects multimodal neurons that map visual features to corresponding text by scoring neurons using gradients, thereby identifying concepts introduced into the model's residual stream.

Additionally, we compare our method with the scoring approach proposed by Pan et al. [6] (abbreviated as Pan's), which utilizes activation values and FFN layer weights.

Using these methods, neurons are scored and averaged across image token positions. The neurons are then sorted in descending order of score, and the top $|N_k|$ neurons are selected for comparison against our method.

C. Identifying Knowledge Neurons

Following the methodology described in II-C, we identify knowledge neurons. Figure 2 illustrates the distribution of neurons identified as knowledge neurons across layers for all knowledge instances in the dataset.

Our identified neurons are primarily concentrated in the middle-to-later layers, while Schwettmann’s neurons tend to be more concentrated in the earlier layers, and Pan’s neurons are heavily concentrated in the final layer.

To conduct a more in-depth analysis, we perform the following experiments.

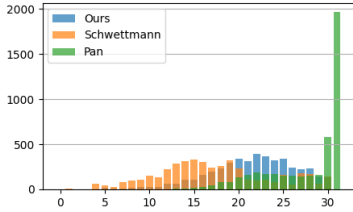


Fig. 2: Layer distribution of identified neurons

D. Are the identified knowledge neurons related to the target knowledge?

We examine whether the identified knowledge neurons are sensitive to the target knowledge in terms of the following: the influence of knowledge neurons on the target knowledge (III-D1); the influence of knowledge neurons on other knowledge (III-D1); whether knowledge neurons correspond to visual concepts (III-D2); and whether knowledge neurons correspond to textual concepts (III-D2).

1) *Image Captioning with Noise Perturbation*: We apply noise to the activation values O' of each identified neuron $(Ll, Ui) \in N_k$ across all image token positions and generate captions for all images $I \in D$.

The noise is generated by sampling a vector from a standard normal distribution and scaling it by three different noise levels $n \in \{40, 80, 120\}$, resulting in a noise vector $v \in \mathbb{R}^P$. To account for the randomness of noise sampling, we generate 10 different noise vectors for each noise level and produce 10 captions per level.

The hyperparameters used for caption generation are as follows.

- do_sample = False
- temperature = 1.0
- num_beams = 1
- max_new_tokens = 32
- min_length = 1
- top_p = 0.9
- repetition_penalty = 1
- length_penalty = 1

We generate image captions for all datasets used to identify neuron groups, datasets containing the same knowledge objects, and datasets containing different knowledge objects \bar{k} .

a) *Impact on Target and Other Knowledge*: In this study, we evaluate whether N_k only affects k by applying noise to N_k and checking whether k is absent in the generated caption when an image containing k is input, and whether \bar{k} is present in the generated caption when an image containing \bar{k} is input. If the target knowledge appears in the caption, the score is set to 1; otherwise, it is set to 0.

Since the dataset includes three different images per knowledge instance, three different neuron groups, N_k^1, N_k^2, N_k^3 , are obtained for a given knowledge k . The scores for these neuron groups are averaged and further averaged across noise levels. The score for images containing k is denoted as $S_k \in [0, 1]$, while the score for images not containing k is denoted as $S_{\bar{k}} \in [0, 1]$. Since lower values of S_k indicate that target knowledge was more effectively suppressed, we use $1 - S_k$ to measure suppression effectiveness (S_{se}). Meanwhile, since higher values of $S_{\bar{k}}$ indicate better retention of other knowledge, we use it directly as a measure of knowledge retention (S_{re}). The results are shown in Table II.

As shown in the results, our method achieves the highest scores in both suppressing target knowledge and retaining other knowledge. While Pan’s method achieves the highest retention score, indicating the least impact on other knowledge, its suppression effectiveness is lower, suggesting that Pan’s neurons are not strongly related to any specific knowledge. Conversely, Schwettmann’s method effectively suppresses target knowledge but has lower retention compared to our method, indicating that it affects other knowledge as well.

These findings suggest that observing activation differences is crucial for identifying neurons strongly associated with specific knowledge.

b) *Comparison with Masked Captions*: Here, we quantitatively compare the caption of the image masked by inpainting with those generated under noise perturbation, as shown in Table I.

The purpose of this evaluation is twofold: to verify whether the grammatical structure of captions is preserved under noise perturbation, and to assess how much information about non-target knowledge present in the image is retained. For example, in Table I, Schwettmann’s method generates ungrammatical captions for “bear,” leading to a lower evaluation score, while our method retains non-target knowledge such as “ocean,” “chair,” and “window” for “banana,” resulting in a higher score.

To achieve these evaluation goals, we adopt three widely used NLP metrics: BLEU [22], ROUGE [23], and BERTScore [24]. The results are summarized in Table III.

our method outperforms Schwettmann’s method in all evaluation metrics. Higher BLEU and ROUGE scores suggest that our method is capable of generating captions containing more words from the masked captions. Additionally, a higher BERTScore indicates that the captions generated under noise perturbation retain meanings closer to the masked captions.

While Pan’s scores surpass ours, Table 2 indicates a lower suppression effect, suggesting minimal differences compared to when non-noise is applied, resulting in smaller deviations from the masked captions. The crucial comparison lies with Schwettmann’s, where a notable suppression effect is observed.

Combining these findings with the qualitative examples (Table I) and the quantitative evaluation (Table II), we conclude that our method surpasses baseline methods in suppressing target knowledge while minimizing deviations from the masked captions and maintaining minimal impact on other knowledge.

2) *Tracing Focus of Neurons in Images and Decoding neurons*: In this section, we analyze where the identified neurons respond most strongly in an image and which tokens

k	n	S_{se}			S_{re}			S_{mean}		
		Schwettmann's	Pan's	ours	Schwettmann's	Pan's	ours	Schwettmann's	Pan's	ours
bed	40	0.4890	0.0110	0.7447	0.7723	0.8477	0.8320	0.6306	0.4294	0.7883
	80	0.1667	0.0000	0.9557	0.5310	0.8227	0.7647	0.3488	0.4113	0.8602
	120	0.2333	0.0000	0.9667	0.3370	0.7963	0.6830	0.2852	0.3982	0.8249
bear	40	0.4887	0.0000	0.1110	0.3523	0.8083	0.7723	0.4205	0.4042	0.4416
	80	0.7553	0.1000	0.5443	0.0087	0.7510	0.6767	0.3820	0.4255	0.6105
	120	0.9223	0.2113	0.7887	0.0000	0.7170	0.6077	0.4612	0.4642	0.6982
banana	40	0.0000	0.2220	0.3777	0.7637	0.8413	0.8437	0.3819	0.5316	0.6107
	80	0.3667	0.2890	0.6113	0.4953	0.8337	0.8143	0.4310	0.5614	0.7128
	120	0.3890	0.3110	0.7777	0.3947	0.8333	0.7947	0.3919	0.5722	0.7862
Ave.	-	0.7459	0.3723	0.7714	0.3742	0.7350	0.6957	0.5600	0.5537	0.7335

TABLE II: Evaluation of image caption generation by noise perturbation.

The bottom line shows the values averaged over all k values in D and averaged over the noise levels and averaged across noise levels.

	BLEU	ROUGE-1	ROUGE-L	BERTScore
Schwettmann's	0.3024	0.3910	0.3529	0.8727
Pan's	0.4615	0.5034	0.4392	0.8971
Ours	0.4607	0.5032	0.4374	0.8971

TABLE III: Quantitative comparison with masked captions

Figure 3 illustrates the results of activation heatmap generation and neuron decoding. The images used to identify neurons for each knowledge category are shown on the far left.

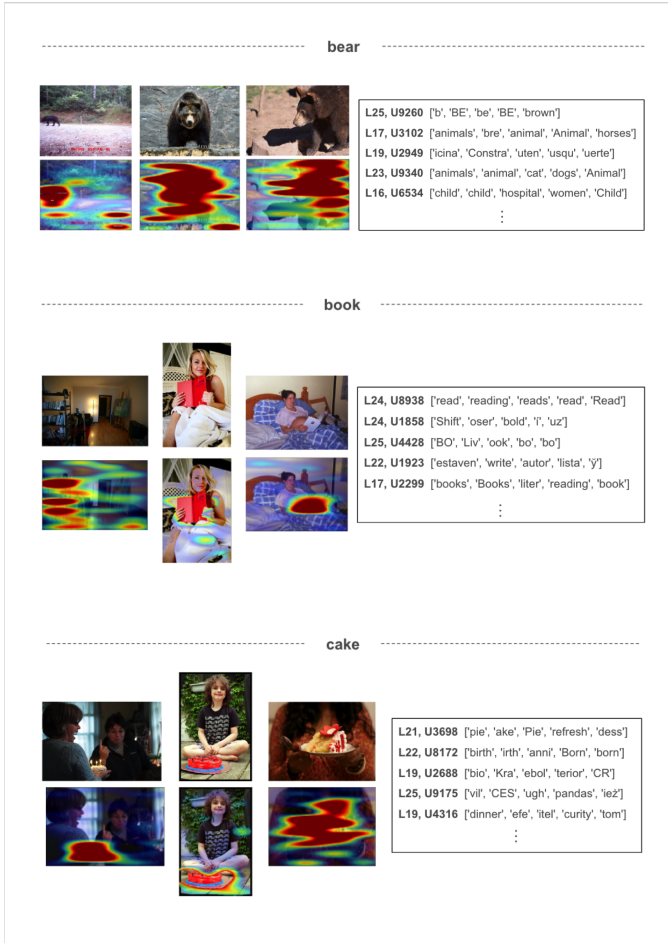


Fig. 3: Activation Heatmap and decoding neurons

IV. RELATED WORK

A. Multimodal Neurons in Pretrained Transformer Language Models

Schwettmann et al. [5] explored the existence and role of multimodal neurons in Transformer models pretrained exclusively on text. Specifically, they combined a frozen Transformer with a self-supervised image encoder and a linear projection layer to analyze how visual information is transformed into textual representations through an image-to-text conversion task. Their study revealed that visual information is not directly converted into textual representations in the early layers of the model. Instead, they identified "multimodal neurons" in the deeper layers that transform visual representations into corresponding textual expressions. Furthermore, their experiments demonstrated that these neurons systematically respond to specific visual concepts and have a causal effect on image caption generation. This research provides insights into how a text-only pretrained model internally processes visual information and utilizes it for text generation, contributing to a deeper understanding of the integration mechanisms between vision and language.

B. Identification and Editing of Multimodal Neurons in Pre-trained Transformers

Pan et al. [6] focused on the internal mechanisms of MLLMs, particularly the identification and modification of neurons that bridge visual and linguistic concepts. The authors scored individual neurons by analyzing the final token of textual inputs and proposed a method based on data sensitivity, specificity, and causality to identify multimodal neurons that influence specific visual knowledge. They introduced a novel approach to efficiently identify key neurons responsible for linking visual and linguistic concepts in caption generation, without requiring gradient computations, which was a limitation of prior methods. Furthermore, they designed a multimodal knowledge editing technique based on the identified neurons to mitigate sensitive words and hallucinations. Through extensive quantitative and qualitative experiments grounded in theoretical assumptions, they validated the effectiveness of their proposed method. This study enhances our understanding of how MLLMs interpret different modalities and integrate cross-modal representations,

providing valuable insights for ongoing improvements in both academia and industry.

V. LIMITATIONS

There are constraints related to the dataset, the model, and the threshold settings.

First, the dataset constraints are threefold: the caption generated when the original image is input must contain the target knowledge; the caption generated when the inpainted image is input must not contain the target knowledge; and the knowledge removed by inpainting must be limited to the target knowledge. These constraints arise from the characteristics of our method, which utilizes activation value differences between the original and inpainted images. If the first constraint is not satisfied due to insufficient model performance, neurons associated with the target knowledge are not initially activated, rendering the activation differences ineffective. Similarly, if the second constraint is not satisfied, neurons related to the target knowledge remain activated even when the inpainted image is input, making the method ineffective. The third constraint is imposed because if the inpainted knowledge object includes non-target knowledge, it becomes impossible to determine which knowledge the activation differences correspond to.

In terms of the model constraints, the only model used in this study is MiniGPT-4 (ViT, LLaMA-2-7B), meaning that the experimental results in III may differ for other MLLMs. In addition, the creation of activation heatmaps is only feasible for MLLMs that adopt an MLP-based vision-language projector and input image tokens independently of text input into the LLM. This is because the operation of scaling activation values at each image token position to the original image size depends on a clear correspondence between each input image token and the patches of the input image. Consequently, architectures that use a Q-former or fuse image and text token representations before inputting them into the LLM do not satisfy this dependency, making heatmap generation infeasible.

The threshold constraints require setting two specific thresholds for each knowledge instance: activation value difference and GradCAM. The values used in this study, extracted from a single sample per knowledge instance, are presented in Table IV. In this study, these values were determined manually; however, future improvements should explore methods for automatic threshold determination.

VI. CONCLUSION

This study takes an initial step toward improving the explainability of Transformer-based text generation models by conducting neuron-level observations using MiniGPT-4, a multimodal large language model (MLLM). We propose a method based on the activation values and gradients of individual neurons at the image token positions in the input sequence.

In text generation experiments with noise perturbation using the MS COCO dataset, our method outperformed Schwettmann’s by approximately 0.17 points and Pan’s by approximately 0.18 points in terms of the average score of knowledge suppression effectiveness and retention rate of other

knowledge. Furthermore, compared to the masked captions, our method partially achieved higher scores than compared methods across BLEU, ROUGE, and BERTScore metrics. These results quantitatively demonstrate that the neurons identified by our method are more strongly related to the target knowledge than to other knowledge and have minimal impact on other knowledge and grammatical ability.

Additionally, by generating activation heatmaps and decoding neurons, we qualitatively show that the identified neurons are indeed related to the target knowledge.

This study has certain limitations regarding dataset usage and model constraints, highlighting the need for further research and expansion.

REFERENCES

- [1] Ashish Vaswani, Noam Shazeer, Niki Parmar, Jakob Uszkoreit, Llion Jones, Aidan N Gomez, Łukasz Kaiser, and Illia Polosukhin. Attention is all you need. In *Advances in neural information processing systems*, pages 5998–6008, 2017.
- [2] Samuel Gehman, Suchin Gururangan, Maarten Sap, Yejin Choi, and Noah A. Smith. RealToxicityPrompts: Evaluating neural toxic degeneration in language models. In Trevor Cohn, Yulan He, and Yang Liu, editors, *Findings of the Association for Computational Linguistics: EMNLP 2020*, pages 3356–3369, Online, November 2020. Association for Computational Linguistics.
- [3] Laura Weidinger, John Mellor, Maribeth Rauh, Conor Griffin, Jonathan Uesato, Po-Sen Huang, Myra Cheng, Mia Glaese, Borja Balle, Atoosa Kasirzadeh, et al. Ethical and social risks of harm from language models. *arXiv preprint arXiv:2112.04359*, 2021.
- [4] Deyao Zhu, Jun Chen, Xiaoqian Shen, Xiang Li, and Mohamed Elhoseiny. Minigpt-4: Enhancing vision-language understanding with advanced large language models, 2023.
- [5] Sarah Schwettmann, Neil Chowdhury, Samuel Klein, David Bau, and Antonio Torralba. Multimodal neurons in pretrained text-only transformers, 2023.
- [6] Haowen Pan, Yixin Cao, Xiaozhi Wang, Xun Yang, and Meng Wang. Finding and editing multi-modal neurons in pre-trained transformers, 2024.
- [7] Kaichen Huang, Jiahao Huo, Yibo Yan, Kun Wang, Yutao Yue, and Xuming Hu. Miner: Mining the underlying pattern of modality-specific neurons in multimodal large language models, 2024.
- [8] Tsung-Yi Lin, Michael Maire, Serge Belongie, Lubomir Bourdev, Ross Girshick, James Hays, Pietro Perona, Deva Ramanan, C. Lawrence Zitnick, and Piotr Dollár. Microsoft coco: Common objects in context, 2015.
- [9] Yizhang Jin, Jian Li, Yexin Liu, Tianjun Gu, Kai Wu, Zhengkai Jiang, Muyang He, Bo Zhao, Xin Tan, Zhenye Gan, Yabiao Wang, Chengjie Wang, and Lizhuang Ma. Efficient multimodal large language models: A survey, 2024.
- [10] Junnan Li, Dongxu Li, Silvio Savarese, and Steven Hoi. Blip-2: Bootstrapping language-image pre-training with frozen image encoders and large language models. In *International conference on machine learning*, pages 19730–19742. PMLR, 2023.
- [11] Jean-Baptiste Alayrac, Jeff Donahue, Pauline Luc, Antoine Miech, Iain Barr, Yana Hasson, Karel Lenc, Arthur Mensch, Katherine Millican, Malcolm Reynolds, et al. Flamingo: a visual language model for few-shot learning. *Advances in neural information processing systems*, 35:23716–23736, 2022.
- [12] Wei-Lin Chiang, Zhuohan Li, Zi Lin, Ying Sheng, Zhanghao Wu, Hao Zhang, Lianmin Zheng, Siyuan Zhuang, Yonghao Zhuang, Joseph E. Gonzalez, Ion Stoica, and Eric P. Xing. Vicuna: An open-source chatbot impressing gpt-4 with 90%* chatgpt quality, March 2023.
- [13] Hugo Touvron, Louis Martin, Kevin Stone, Peter Albert, Amjad Almahairi, Yasmine Babaei, Nikolay Bashlykov, Soumya Batra, Prajjwal Bhargava, Shruti Bhosale, Dan Bikel, Lukas Blecher, Cristian Canton Ferrer, Moya Chen, Guillem Cucurull, David Esiobu, Jude Fernandes, Jeremy Fu, Wenyin Fu, Brian Fuller, Cynthia Gao, Vedanuj Goswami, Naman Goyal, Anthony Hartshorn, Saghar Hosseini, Rui Hou, Hakan Inan, Marcin Kardas, Viktor Kerkez, Madian Khabsa, Isabel Kloumann, Artem Korenev, Punit Singh Koura, Marie-Anne Lachaux, Thibaut Lavril, Jenya Lee, Diana Liskovich, Yinghai Lu, Yuning Mao, Xavier Martinet,

- Todor Mihaylov, Pushkar Mishra, Igor Molybog, Yixin Nie, Andrew Poulton, Jeremy Reizenstein, Rashi Rungta, Kalyan Saladi, Alan Schelten, Ruan Silva, Eric Michael Smith, Ranjan Subramanian, Xiaoqing Ellen Tan, Binh Tang, Ross Taylor, Adina Williams, Jian Xiang Kuan, Puxin Xu, Zheng Yan, Iliyan Zarov, Yuchen Zhang, Angela Fan, Melanie Kambadur, Sharan Narang, Aurelien Rodriguez, Robert Stojnic, Sergey Edunov, and Thomas Scialom. Llama 2: Open foundation and fine-tuned chat models, 2023.
- [14] Alexey Dosovitskiy, Lucas Beyer, Alexander Kolesnikov, Dirk Weissenborn, Xiaohua Zhai, Thomas Unterthiner, Mostafa Dehghani, Matthias Minderer, Georg Heigold, Sylvain Gelly, Jakob Uszkoreit, and Neil Houlsby. An image is worth 16x16 words: Transformers for image recognition at scale, 2021.
- [15] Mor Geva, Roei Schuster, Jonathan Berant, and Omer Levy. Transformer feed-forward layers are key-value memories. *CoRR*, abs/2012.14913, 2020.
- [16] Mor Geva, Avi Caciularu, Kevin Wang, and Yoav Goldberg. Transformer feed-forward layers build predictions by promoting concepts in the vocabulary space. In Yoav Goldberg, Zornitsa Kozareva, and Yue Zhang, editors, *Proceedings of the 2022 Conference on Empirical Methods in Natural Language Processing*, pages 30–45, Abu Dhabi, United Arab Emirates, December 2022. Association for Computational Linguistics.
- [17] Kevin Meng, David Bau, Alex J Andonian, and Yonatan Belinkov. Locating and editing factual associations in GPT. In Alice H. Oh, Alekh Agarwal, Danielle Belgrave, and Kyunghyun Cho, editors, *Advances in Neural Information Processing Systems*, 2022.
- [18] Damai Dai, Li Dong, Yaru Hao, Zhifang Sui, Baobao Chang, and Furu Wei. Knowledge neurons in pretrained transformers. In Smaranda Muresan, Preslav Nakov, and Aline Villavicencio, editors, *Proceedings of the 60th Annual Meeting of the Association for Computational Linguistics (Volume 1: Long Papers)*, pages 8493–8502, Dublin, Ireland, May 2022. Association for Computational Linguistics.
- [19] Xiaozhi Wang, Kaiyue Wen, Zhengyan Zhang, Lei Hou, Zhiyuan Liu, and Juanzi Li. Finding skill neurons in pre-trained transformer-based language models. In Yoav Goldberg, Zornitsa Kozareva, and Yue Zhang, editors, *Proceedings of the 2022 Conference on Empirical Methods in Natural Language Processing*, pages 11132–11152, Abu Dhabi, United Arab Emirates, December 2022. Association for Computational Linguistics.
- [20] Alexandru Telea. An image inpainting technique based on the fast marching method. *Journal of Graphics Tools*, 9(1):23–34, 2004.
- [21] Ramprasaath R. Selvaraju, Michael Cogswell, Abhishek Das, Ramakrishna Vedantam, Devi Parikh, and Dhruv Batra. Grad-cam: Visual explanations from deep networks via gradient-based localization. In *Proceedings of the IEEE International Conference on Computer Vision (ICCV)*, Oct 2017.
- [22] Kishore Papineni, Salim Roukos, Todd Ward, and Wei-Jing Zhu. Bleu: a method for automatic evaluation of machine translation. In Pierre Isabelle, Eugene Charniak, and Dekang Lin, editors, *Proceedings of the 40th Annual Meeting of the Association for Computational Linguistics*, pages 311–318, Philadelphia, Pennsylvania, USA, July 2002. Association for Computational Linguistics.
- [23] Chin-Yew Lin. ROUGE: A package for automatic evaluation of summaries. In *Text Summarization Branches Out*, pages 74–81, Barcelona, Spain, July 2004. Association for Computational Linguistics.
- [24] Tianyi Zhang, Varsha Kishore, Felix Wu, Kilian Q. Weinberger, and Yoav Artzi. BERTscore: Evaluating text generation with bert, 2020.

APPENDIX







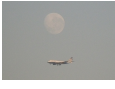























k	image	variable	value	k	image	variable	value	k	image	variable	value
banana		$threshold_a$	2.5	bed		$threshold_a$	1.5	bear		$threshold_a$	1.0
		$threshold_g$	0.0003			$threshold_g$	0.0005			$threshold_g$	0.0005
giraffe		$threshold_a$	1.5	pizza		$threshold_a$	1.5	bus		$threshold_a$	1.5
		$threshold_g$	0.0002			$threshold_g$	0.0003			$threshold_g$	0.0001
airplane		$threshold_a$	2	horse		$threshold_a$	1.0	refrigerator		$threshold_a$	1.25
		$threshold_g$	0.0			$threshold_g$	0.0007			$threshold_g$	0.0005
toilet		$threshold_a$	1.5	tennis racket		$threshold_a$	1.5	fire hydrant		$threshold_a$	1.5
		$threshold_g$	0.0001			$threshold_g$	0.0001			$threshold_g$	0.0005
stop sign		$threshold_a$	1.0	microwave		$threshold_a$	1.0	bicycle		$threshold_a$	1.5
		$threshold_g$	0.00075			$threshold_g$	0.0002			$threshold_g$	0.0004
cake		$threshold_a$	1.25	toaster		$threshold_a$	1.0	surfboard		$threshold_a$	1.5
		$threshold_g$	0.0003			$threshold_g$	0.001			$threshold_g$	0.0003
snowboard		$threshold_a$	1.5	traffic light		$threshold_a$	2.0	keyboard		$threshold_a$	1.0
		$threshold_g$	0.002			$threshold_g$	0.0002			$threshold_g$	0.0005
cell phone		$threshold_a$	1.5	scissors		$threshold_a$	1.0	book		$threshold_a$	1.5
		$threshold_g$	0.0005			$threshold_g$	0.002			$threshold_g$	0.0001
clock		$threshold_a$	2.0	suitcase		$threshold_a$	1.2	backpack		$threshold_a$	1.0
		$threshold_g$	0.0005			$threshold_g$	0.0007			$threshold_g$	0.001
umbrella		$threshold_a$	0.8	laptop		$threshold_a$	1	vase		$threshold_a$	1
		$threshold_g$	0.0015			$threshold_g$	0.00075			$threshold_g$	0.0007

TABLE IV: Thresholds of activation differences and GradCAM(one excerpt of each knowledge)

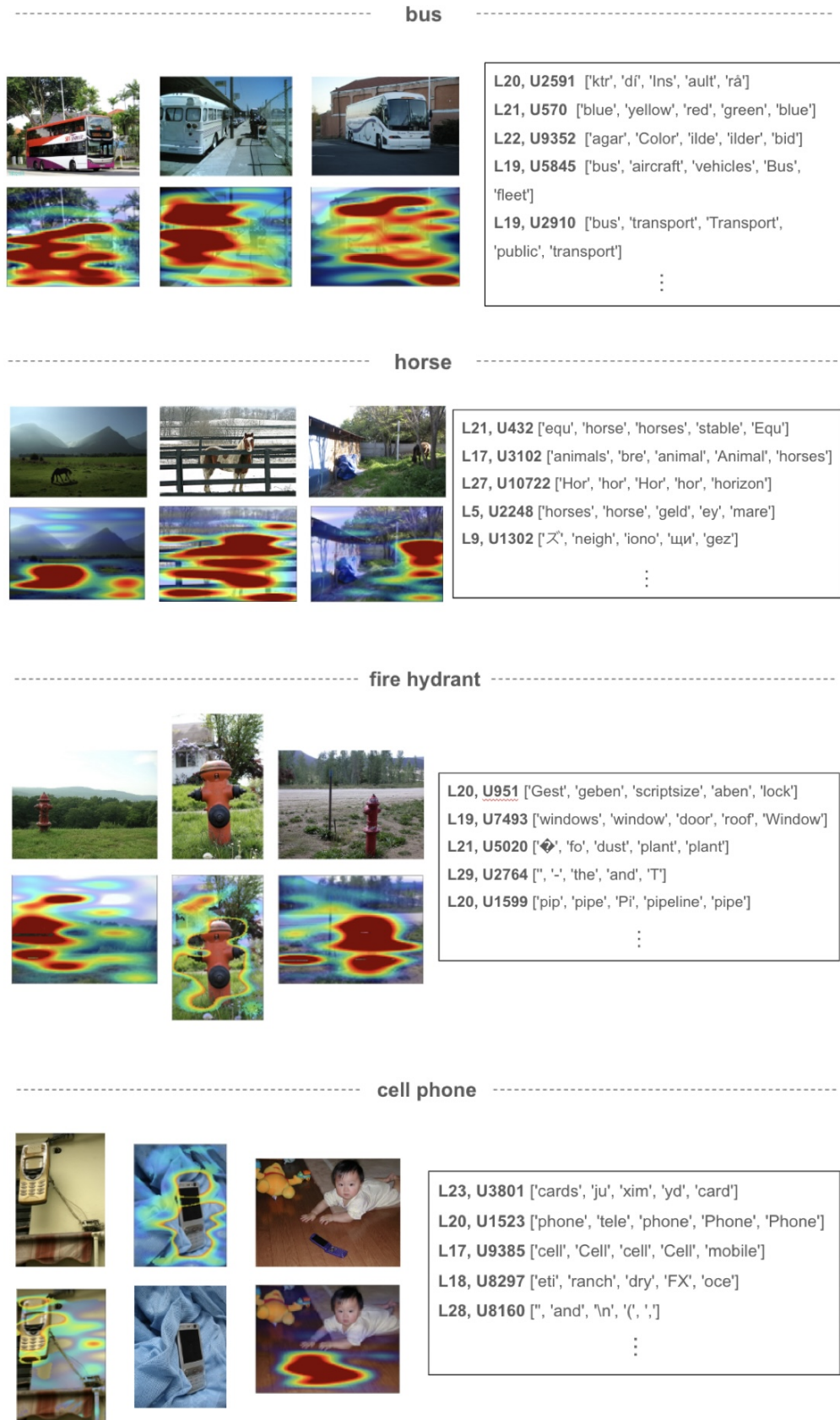


Fig. 4: Activation heatmap and Decoding neurons

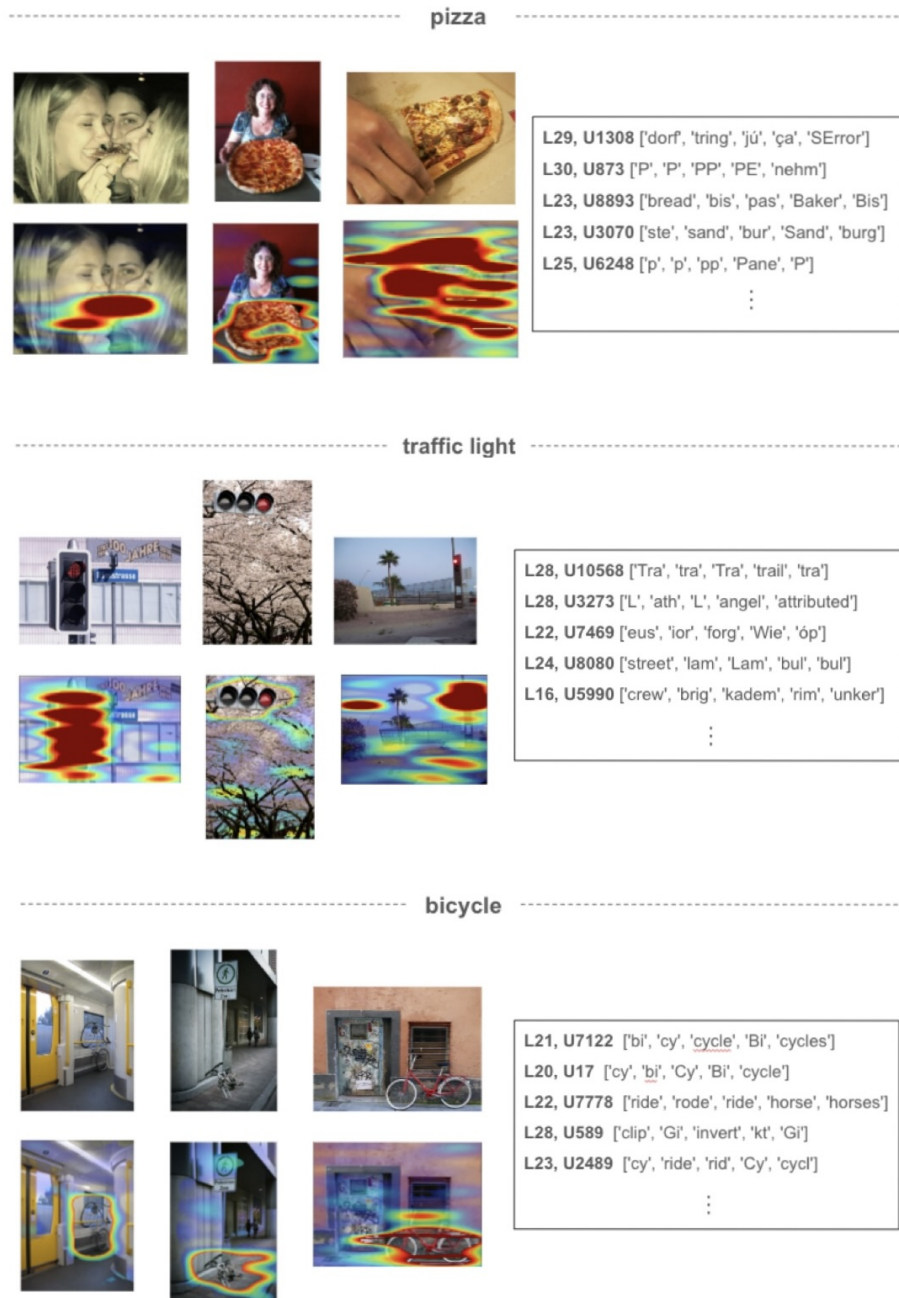


Fig. 5: Activation heatmap and Decoding neurons